Supporting Information

Impact of Fullerene Derivative Isomeric Purity on the Performance of Inverted Planar Perovskite Solar Cells

*Edison Castro, Gerardo Zavala, Sairaman Seetharaman, Francis D'Souza, and Luis Echegoyen**

E. Castro, E. G. Zavala, Prof. L. Echegoyen
Department of Chemistry
University of Texas at El Paso
El Paso, Texas, 79968, United States
E-mail: echegoyen@utep.edu

S. Seetharaman, Prof. F. D'Souza
Department of Chemistry
University of North Texas
Denton, TX 76203-5017, United States.

General Methodology

All chemicals were reagent grade, purchased from Sigma Aldrich. Silica gel (Redisep silica, 40-60 μ, 60 Å) was used to separate the products from the pristine fullerene. HPLC experiments were performed on an LC-9130NEXT apparatus (Japan Analytical Industry Co. Ltd.) monitored using a UV detector at 320 nm, and toluene as eluent. MALDI-TOF mass spectrometric measurements were conducted on a Bruker Microflex LRF mass spectrometer on reflector positive mode. The NMR spectra were recorded using a JEOL 600 MHz spectrometer. The UV/Vis-NIR spectra were taken using a Cary 5000 UV/Vis-NIR spectrophotometer using chloroform solutions. Cyclic voltammetry (CV) experiments were carried out under an Argon atmosphere at room temperature using a CH Instrument Potentiostat. Scan rate for CV experiments was 100 mV/s. A one compartment cell with a

standard three-electrode set up was used, consisting of a 1 mm diameter glassy carbon disk as the working electrode, a platinum wire as the counter electrode and a silver wire as the pseudo-reference electrode, in a solution of anhydrous *o*-DCB containing 0.05 M n-Bu_4NPF_6. Ferrocene was added to the solution at the end of each experiment as an internal standard.

Experimental Section

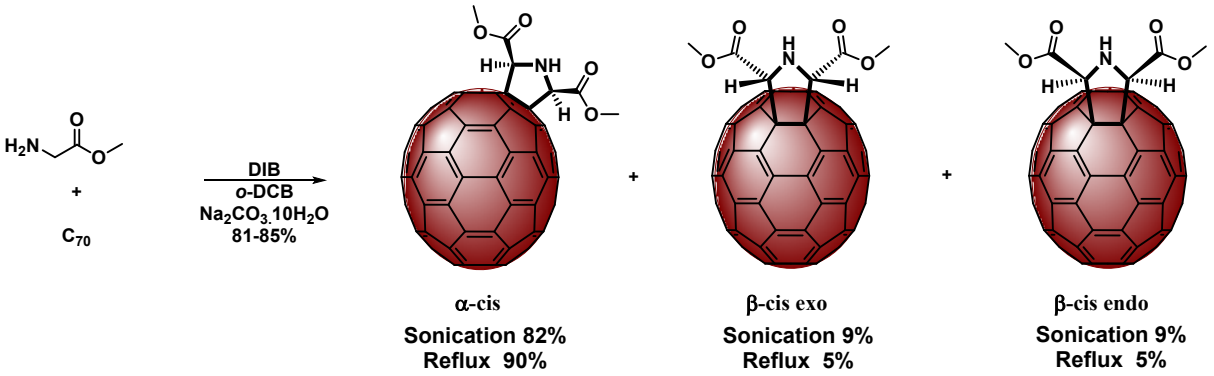

Scheme S1. Synthesis of $DMEC_{70}$ fullerene derivatives. The structures of the chiral α-type isomer (left) and the two possible achiral β-type isomers (right). The percentage was calculated from 3 independent reactions.

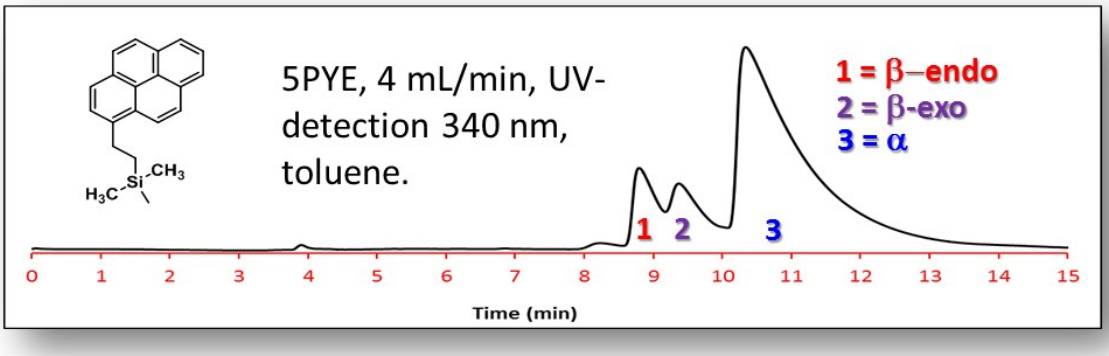

Figure S1. HPLC chromatogram of the C_{70} *mono*-adducts regioisomeric mixture.

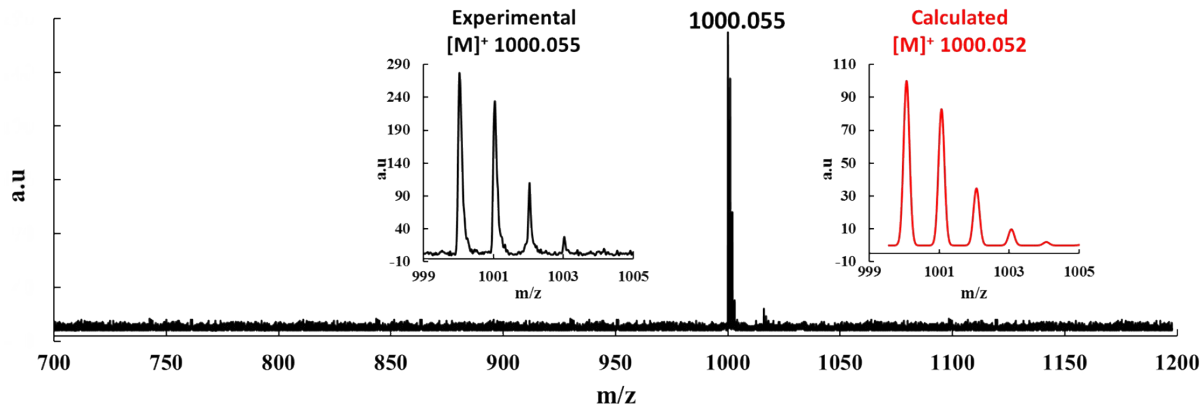

Figure S2. MALDI-TOF spectrum of $DMEC_{70}$ using 1,8,9-trihydroxyanthracene (THA) as matrix C_{70}.

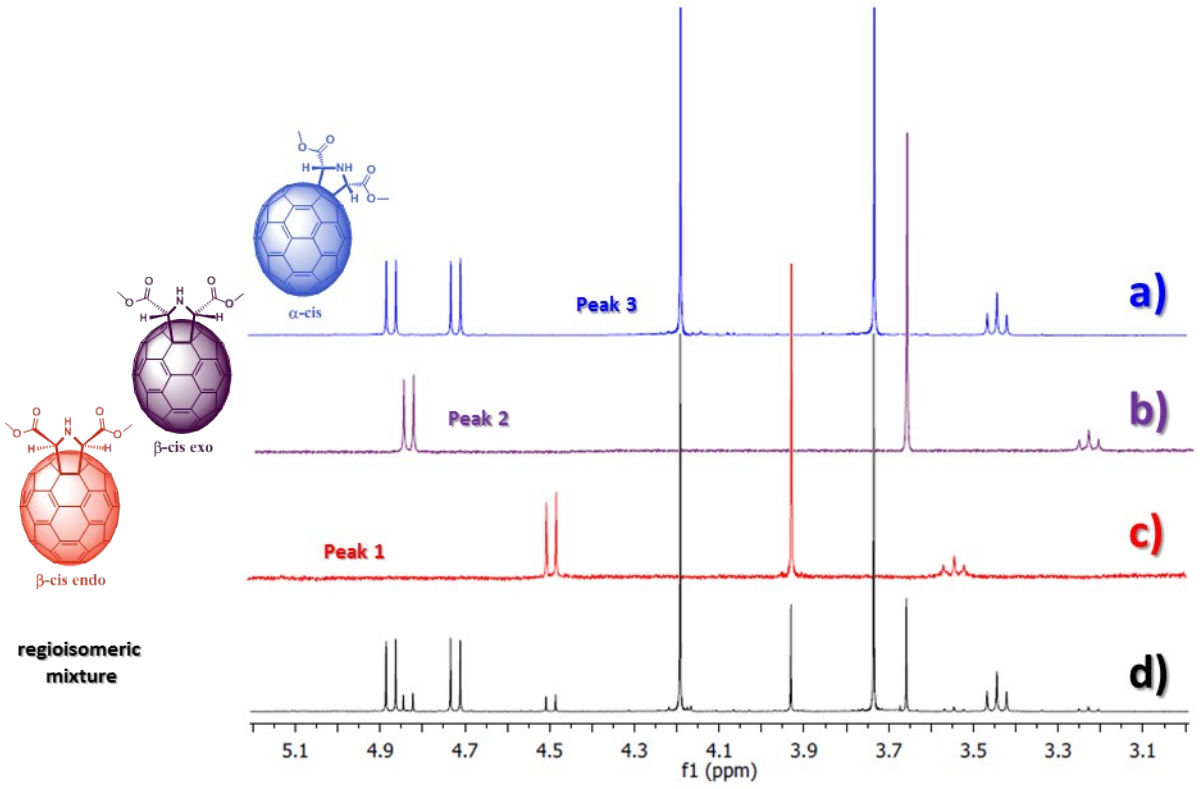

Figure S3. ^{1}H-NMR of the $DMEC_{70}$ fullerene derivatives, before and after HPLC purification ($CDCl_3$, 298 K, 600 MHz). a) α-cis b) β-cis exo c) β-cis endo d) regioisomeric mixture.

α-$DMEC_{70}$ ^{1}H NMR (600 MHz; $CDCl_3$, 298 K) δ (ppm) 4.89 (*d*, J = 13.7 Hz, 1 H, α-CH), 4.73 (*d*, J = 13.8 Hz, 1 H, α-CH), 4.20 (*s*, 3 H, α-CH_3), 3.75 (*s*, 3 H, α-CH_3), 3.46 (*t*, J = 13.8 Hz, 1 H, α-NH).

β-exo-DMEC$_{70}$ ^{1}H NMR (600 MHz; $CDCl_3$, 298 K) δ (ppm) 4.84 (*d*, J = 13.7 Hz, 2 H, β-CH), 3.67 (*s*, 6 H, β-CH_3), 3.24 (*t*, J = 13.7 Hz, 1 H, β-NH).

β-endo-DMEC$_{70}$ ^{1}H NMR (600 MHz; $CDCl_3$, 298 K) δ (ppm) 4.51 (*d*, J = 13.7 Hz, 2 H, β-CH), 3.94 (*s*, 6 H, β-CH_3), (*t*, J = 13.7 Hz, 1 H, β-NH).

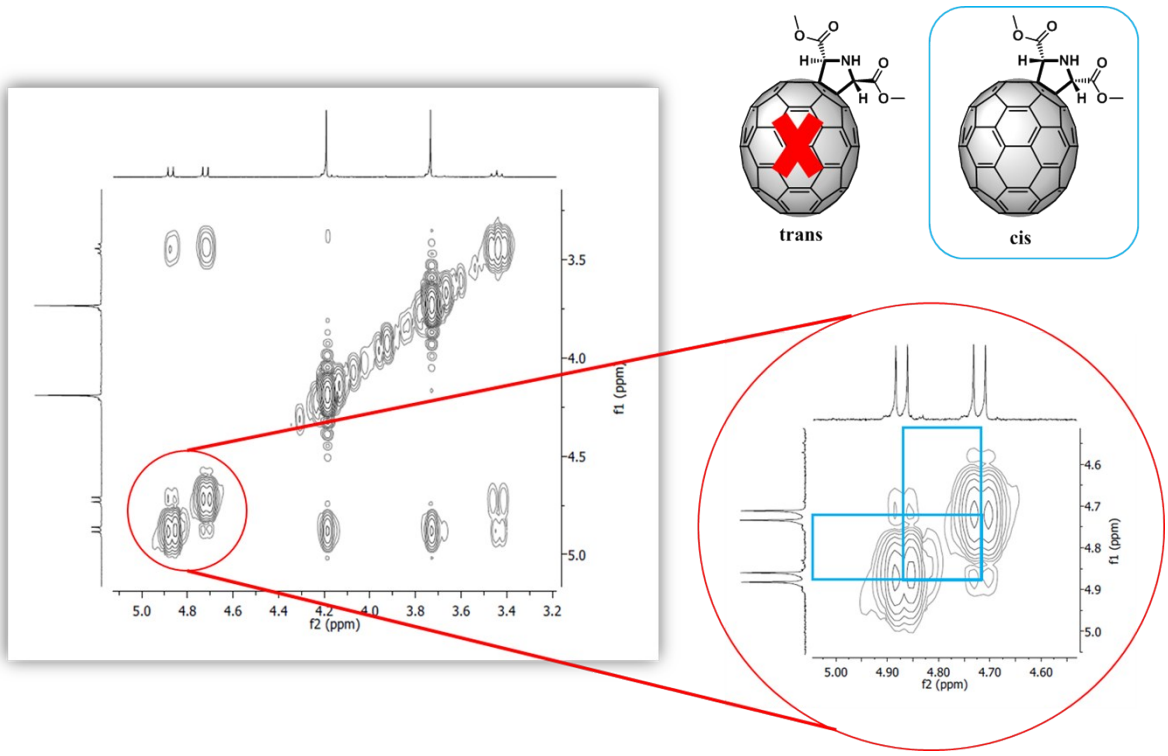

Figure S4. NOESY of the α-DMEC$_{70}$ isomer.

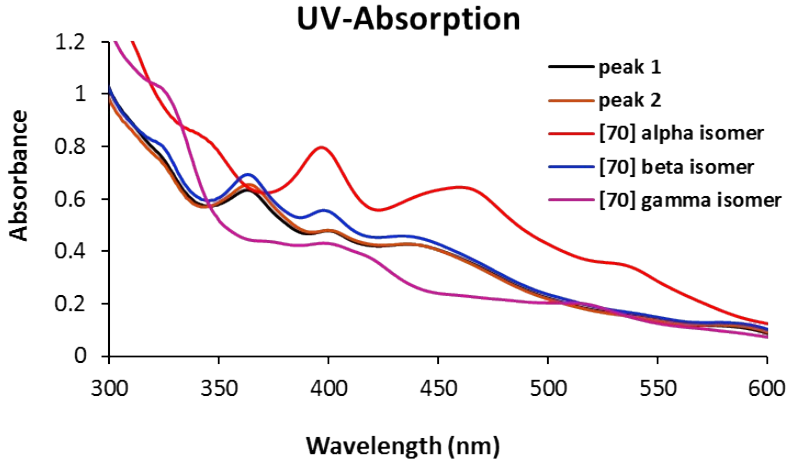

Figure S5. UV-Vis spectra of β-endo-DMEC$_{70}$ (peak 1), β-exo-DMEC$_{70}$ (peak 2), α-pyrrolidine-C$_{70}$, β-pyrrolidine-C$_{70}$ and γ-pyrrolidine-C$_{70}$ in chloroform.

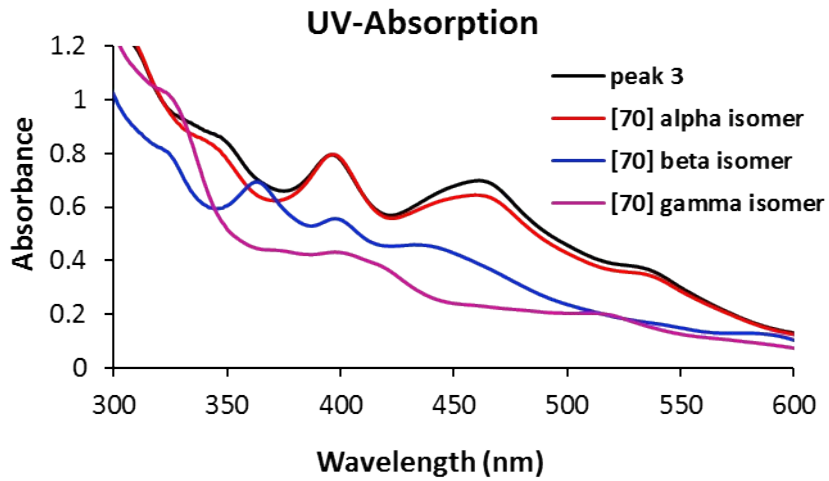

Figure S6. UV-Vis spectra of α-exo-DMEC$_{70}$ (peak 3), α-pyrrolidine-C$_{70}$, β-pyrrolidine-C$_{70}$ and γ-pyrrolidine-C$_{70}$ in chloroform.

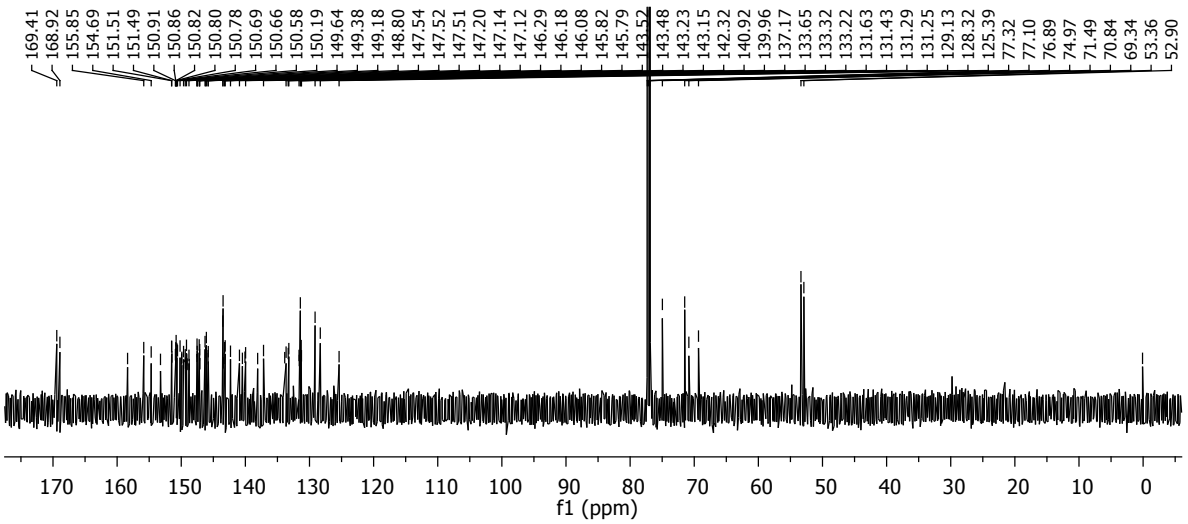

Figure S7. ^{13}C NMR (150 MHz; $CDCl_3$, 298 K) of α-DMEC$_{70}$.

^{13}C NMR (150 MHz; $CDCl_3$, 298 K) δ (ppm) 169.4, 168.9, 158.4, 155.9, 154.7, 153.2, 151.5, 151.5, 151.5, 150.9, 150.9, 150.8, 150.8, 150.8, 150.7, 150.7, 150.6, 150.2, 150.1, 149.9,

149.9, 149.6, 149.4, 149.3, 149.2, 149.1, 149.1, 149.1, 148.8, 148.8, 147.5, 147.5, 147.5, 147.2, 147.1, 147.1, 147.1, 147.0, 146.3, 146.2, 146.1, 146.0, 145.8, 145.8, 143.5, 143.5, 143.4, 143.3, 143.2, 143.2, 142.3, 140.9, 140.5, 140.1, 140.0, 138.1, 137.2, 133.9, 133.7, 133.3, 133.2, 131.6, 131.6, 131.4, 131.3, 131.3, 129.1, 128.3, 125.4, 75.0, 71.5, 70.8, 69.3, 53.4, 52.9.

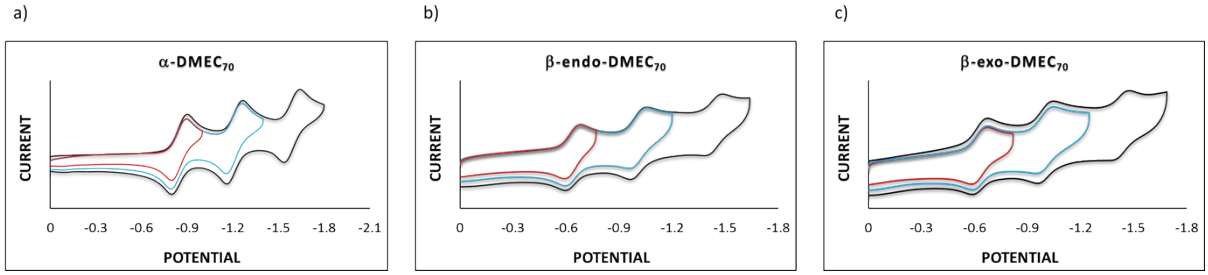

Figure S8. Cyclic voltammetry of a) α-$DMEC_{70}$ b) β-endo-$DMEC_{70}$ and c) β-exo-$DMEC_{70}$ (*o*-DCB containing 0.05 M *n*-Bu_4NPF_6; using the redox couple Fc/Fc^+ as internal reference).

Device characterization: *J-V* characteristics of photovoltaic cells were tested using a Keithley 2420 source meter under a Photo Emission Tech SS100 Solar Simulator, and the light intensity was calibrated by a standard Si solar cell. EQEs were measured using a Bentham (from Bentham Instruments Ltd) measurement system. The light intensity was calibrated using a single-crystal Si photovoltaic cell as the reference. The *J-V* and EQE measurements were carried out in air. The SEM images were collected using a ZEISS Sigma FE-SEM, where the electron beam was accelerated in the range of 500 V to 30 kV. Film thicknesses were measured using a KLA Tencor profilometer. The contact angles of water were determined using a Ramé-Hart model 250 goniometer using pure deionized water at room temperature at a constant volume of 5 µL. A total of ten static measurements were analyzed and averaged for each ETL. The stead-state photoluminescence spectra were recorded on a Horiba Yvon Nanolog spectrometer coupled with a time-correlated single photon counting (TCSPC) with nanoLED excitation sources for time-resolved emission measurements.

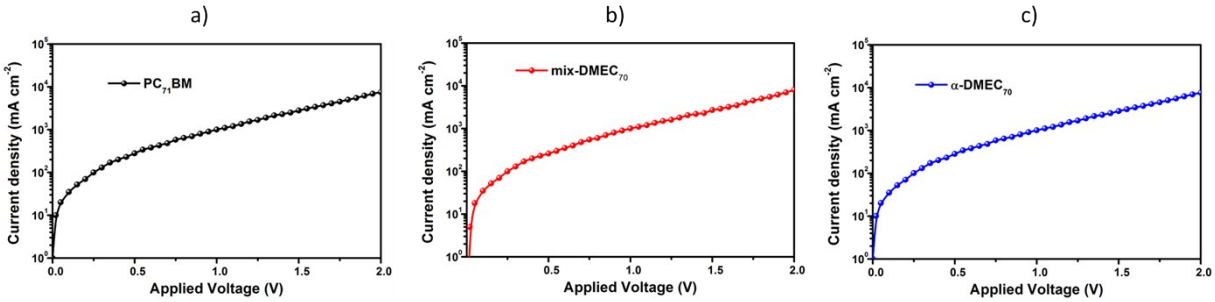

Figure S9. Measured space-charge limited *J-V* characteristics of a) $PC_{71}BM$, b) mix-$DMEC_{70}$ and c) α-$DMEC_{70}$ for electron only devices with ITO/Al/fullerene/Al structure.

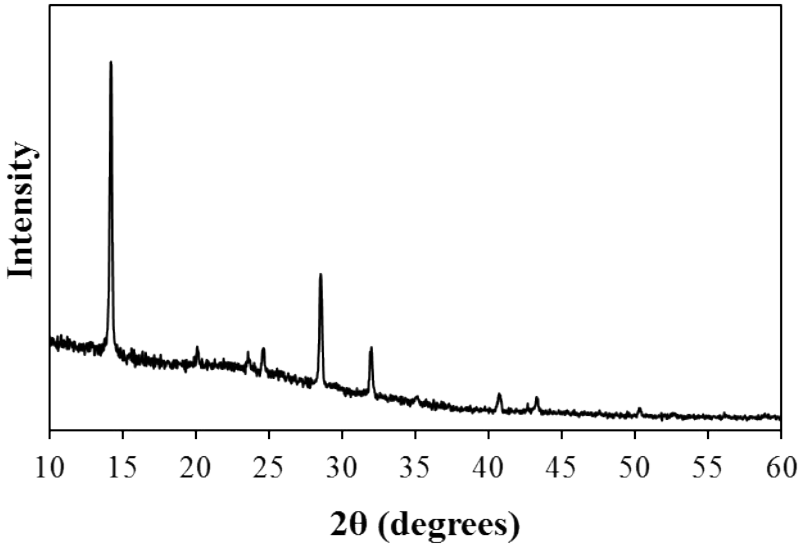

Figure S10. The XRD spectra of the perovskite films.

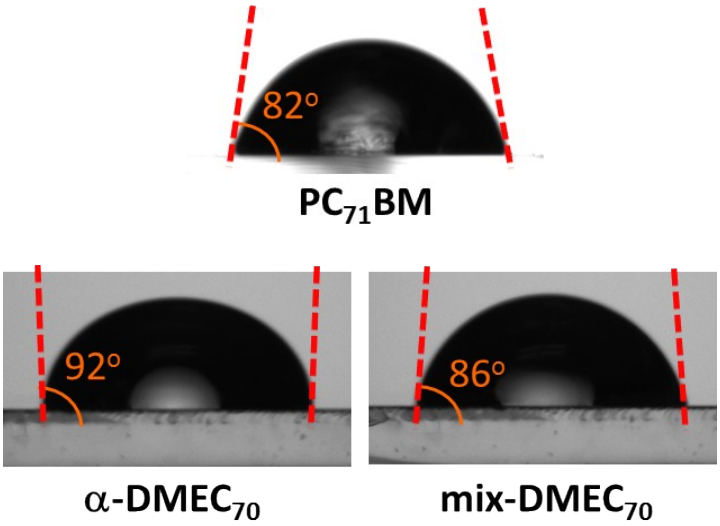

Figure S11. Images of the water droplet contact angles on the surfaces of $PC_{71}BM$, α-$DMEC_{70}$ and mix-$DMEC_{70}$ thin films.

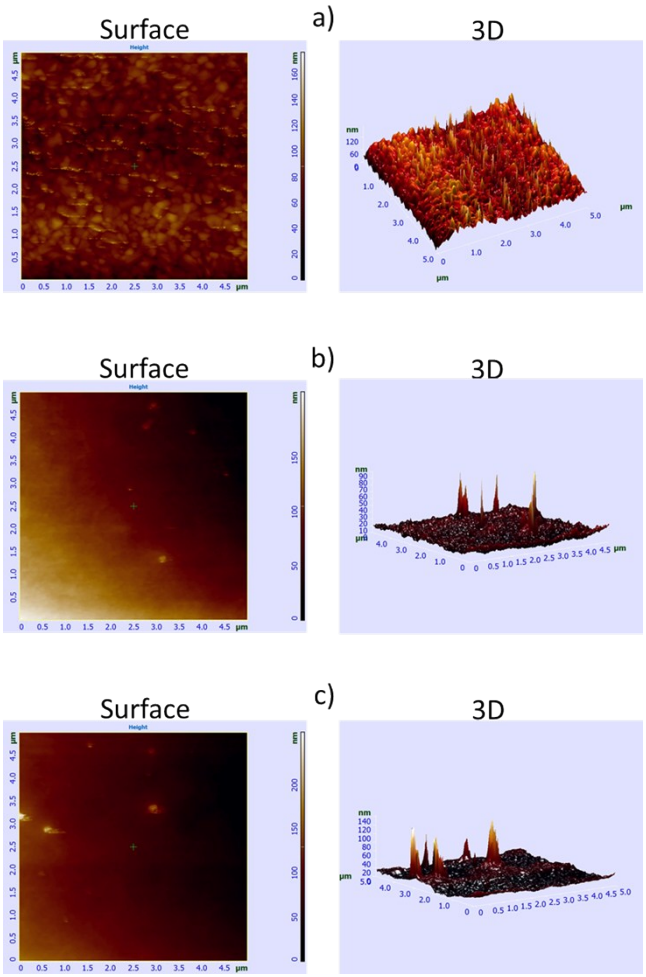

Figure S12. AFM Images of a) perovskite layer, b) mix-$DMEC_{70}$ deposited on top of the perovskite layer and d) α-$DMEC_{70}$ deposited on top of the perovskite layer.